Full-Zone Spin Splitting for Electrons and Holes in Bulk GaAs and GaSb

Jun-Wei Luo, Gabriel Bester,* and Alex Zunger†
National Renewable Energy Laboratory, Golden, Colorado 80401, USA
(Received 12 September 2008; published 5 February 2009)

The spin-orbit interaction—a fundamental electroweak force—is equivalent to an effective magnetic field intrinsic to crystals, leading to band spin splitting for certain k points in sufficiently low-symmetry structures. This (Dresselhaus) splitting has usually been calculated at restricted regions in the Brillouin zone via small wave vector approximations (e.g., $\mathbf{k}\cdot\mathbf{p}$), potentially missing the "big picture." We provide a full-zone description of the Dresselhaus splitting in zinc blende semiconductors by using pseudopotentials, empirically corrected to rectify local density approximation errors by fitting GW results. In contrast to what was previous thought, we find that the largest spin splitting in the lowest conduction band and upper valence band (VB1) occurs surprisingly along the (210) direction, not the (110) direction, and that the splitting of the VB1 is comparable to that of the next two valence bands VB2 and VB3.

DOI: 10.1103/PhysRevLett.102.056405 PACS numbers: 71.20.Nr, 71.15.Rf, 71.70.Ej

The relativistic interaction between spin and orbit creates an *internal* magnetic field B_{eff} in periodic solids [1–3],

$$B_{\text{eff}} = \frac{\hbar}{2m^2c^2g\mu_B}[\nabla V(\mathbf{r}) \times \mathbf{p}], \tag{1}$$

where $V(\mathbf{r})$ is the crystal potential and $\mathbf{p}$ is the momentum. This can cause a lifting of the degeneracy between spin-up $\varepsilon^{\uparrow}_{i,\mathbf{k}}$ and spin-down $\varepsilon^{\downarrow}_{i,\mathbf{k}}$ states of band i at wave vector $\mathbf{k}$, called intrinsic (Dresselhaus [1]) spin splitting $\Delta_i(\mathbf{k})$. This splitting is nonzero only for certain crystal symmetries and certain wave vectors. For example, in the diamondlike structure with its inversion symmetry ($Fd\bar{3}m$), the bands at all $\mathbf{k}$ points lack spin splitting, whereas in the noncentrosymmetry $F\bar{4}3m$ zinc blende space group only certain points in the fcc Brillouin zone—Γ, Δ, Λ_6, L, and X—lack spin splitting by symmetry. Traditionally, this bulk-intrinsic spin splitting [1] has been studied mostly in the close vicinity near the Brillouin zone center $\mathbf{k}_0 = \Gamma$ [4–6], or at some band edges, e.g., $\mathbf{k}_0 = L$ [7,8] or $\mathbf{k}_0 = X$ [8,9]. This tradition is anchored in the ubiquitous use in the literature of small wave vector expansion models such as effective mass approximation (EMA) or $\mathbf{k}\cdot\mathbf{p}$ [5,7–9], limited not only in the narrow range $\Delta\mathbf{k}$ around $\mathbf{k}_0$, but also requiring the often difficult-to-compute $\mathbf{k}\cdot\mathbf{p}$ parameters (e.g., interband coupling) for different Brillouin zone valleys $\mathbf{k_0} = \Gamma, X, L$ and different interacting bands. In the EMA, the Dresselhaus and Rashba terms are parameters, directly fitted to experiment, so no new information is revealed. These limitations could be circumvented if one focuses instead on the crystal potential $V(\mathbf{r})$ that produces via diagonalization of $\frac{1}{2}\nabla^2 + V(\mathbf{r})$ the all-band, full-zone band eigenvalues and hence spin splitting $\Delta_i(\mathbf{k})$. Here we inquire about the spin splitting of common bulk semiconductors throughout the Brillouin zone and for many $i =$ valence and $i =$ conduction bands. We use (pseudopotential, plane-wave) band theory in which the fundamental, parametrized quantity is the crystal potential $V(\mathbf{r})$ and a parametrized spin-orbit interaction rather than $\mathbf{k}\cdot\mathbf{p}$ parameters. This approach automatically includes coupling between any number of bands, any number of interacting valleys, and is naturally unlimited in the range of validity $\Delta\mathbf{k}$ around any particular $\mathbf{k}_0$. The results $\Delta_i(\mathbf{k})$ can then be fit, e.g., to a power series in $|\mathbf{k}|$ (analogous [1] to $\mathbf{k}\cdot\mathbf{p}$ but valid at any $\mathbf{k}_0$), thus providing a more accurate reference point for $\mathbf{k}\cdot\mathbf{p}$ results. This approach shifts, however, the burden of correctly encoding the "personality" of a given material from "$\mathbf{k}\cdot\mathbf{p}$ parameters" into its underlying crystal potential $V(\mathbf{r})$. Whereas, not surprisingly, describing $V(\mathbf{r})$ via the local density approximation (LDA) is insufficiently accurate on account of underestimating band gaps [6] by $\approx$60% and underestimating effective masses by $\approx$40% leading to overestimation of its spin splitting [6], better approximations, such as GW [6] are sufficient for most purposes. Here, we construct the crystal potential $V(\mathbf{r})$ as a superposition of screened (overlapping) spherical atomic pseudopotential $\hat{v}_\alpha(\mathbf{r})$ parametrized so as to remove the LDA band gap error and reproduce closely GW results for the bulk solid. Although the GW method can yield the spin splitting at arbitrary points in the Brillouin zone, we are interested here in a method that can be applied to both bulk solids, as well as to quantum wells ($\sim$100 atoms/cell) and to quantum dots ($\sim$1 000 000 atoms/cell). The atomistic pseudopotential method has been applied to all such systems before [10–14]. Alas, GW cannot be applied practically to any truly large system. Thus, our strategy is to map existing GW calculations on pseudopotential for the Brillouin zone directions available. Although fitting a finite number of directions does not automatically guarantee that other directions will be reproduced well, our experience with our pseudopotential is that fitting is required only at a few points to yield a globally robust behavior. In this Letter we use such a description to get a glimpse at the full-zone spin splitting of few valence bands and few conduction bands of GaAs and GaSb. In contrast to what was previ-

ously thought, we find that the largest spin splitting in the lowest conduction band (CB1) and upper valence band (VB1) occurs surprisingly along the (210) direction, not the (110) direction, and that the splitting of the VB1 is comparable to that of the next two valence bands VB2 and VB3.

Crystal pseudopotential.—The band structure of bulk material is obtained via direct diagonalization of the single-particle Schrödinger equation in an empirical pseudopotential method (EPM) [15] representation,

$$\left(-\frac{1}{2}\nabla^2 + V(\mathbf{r})\right)\psi_i(\mathbf{r}) = E_i\psi_i(\mathbf{r}). \quad (2)$$

The crystal potential $V(\mathbf{r}) = \sum_{n,\alpha}\hat{v}_\alpha(\mathbf{r} - \mathbf{R}_{n,\alpha})$ is a superposition of screened atomic potentials $\hat{v}_\alpha$ of atom type α located at atomic site $\mathbf{R}_{n,\alpha}$ which contains a local part v_α^L and a nonlocal spin-orbit interaction part $\hat{v}_\alpha^{\mathrm{NL}}$. The nonlocal spin-orbit interaction $\hat{v}_\alpha^{\mathrm{NL}}$ is described by a Kleinman-Bylander separable form [16]

$$\hat{v}_\alpha^{\mathrm{NL}} = \beta_\alpha \sum_{i,j} |i\rangle B(i,j)\langle j|, \quad (3)$$

where $|i\rangle$ and $|j\rangle$ are reference functions, and $B(i, j)$ is a matrix representation of the spin-orbit interaction: $B(i, j) = \langle i|\mathbf{L}\cdot\mathbf{S}|j\rangle$, where $\mathbf{L}$ and $\mathbf{S}$ are the spatial angular momentum operator and spin operator, respectively. The pseudopotentials $\hat{v}_\alpha$ are fitted [17,18] to experimental transition energies, effective masses, and deformation potentials of the bulk material. The supplementary section [18] describes the fit in detail. The wave function $\psi_i(\mathbf{r})$ is expanded by a set of plane waves. Table I gives the critical properties calculated by our standard empirical pseudopotential (EP-I) used previously [14,17]. Although this potential was not fit to the spin splitting, it gives a good representation of the *GW* results [Fig. 1(a)]. In fact, writing $\Delta_{\mathrm{CB1}}(\mathbf{k}) = \gamma_c|\mathbf{k}|^3$ we get from our standard EP-I $\gamma_c = 5.7$ (γ_c is in eV Å^3) whereas *GW* [6] gives $\gamma_c = 8.5$, a big improvement over LDA [21] that gives $\gamma_c = 46.8$ [Fig. 1(c)]. Over the full extent of the data shown in Fig. 1, the agreement between LDA and *GW* is qualitatively good, except near Γ. Indeed, LDA is known to fail for band gaps and for effective masses more dramatically near Γ than in other regions in the zone (see Ref. [6]). Experimental values are indirect and somewhat scattered and are 9.0 [20], 11.0 [20], and 17–35 [20].

It is possible to further improve EP-I [see black line in Fig. 1(b)]. Analysis of the spin splitting [5] reveals that it depends on (1) the energy splittings due to spin-orbit interaction [e.g., $\Delta_0 = E(\Gamma_{8v}) - E(\Gamma_{7v})$, $\Delta_0' = E(\Gamma_{8c}) - E(\Gamma_{7c})$, and $\Delta_1 = E(L_{4,5v}) - E(L_{6v})$], (2) the position of the two lowest-lying conduction band levels at Γ [i.e., $E_0 = E(\Gamma_{6c}) - E(\Gamma_{8v})$ and $E_0' = E(\Gamma_{7c}) - E(\Gamma_{8v})$], and (3) on matrix elements of the momentum operator and spin-orbit operator. The latter depends on the wave functions. Thus, even if we have a pseudopotential which fits well the energy levels [Δ_0, Δ_0', Δ_1, E_0, and E_0', i.e., items (1) and (2) above], it may not give accurate spin splittings, unless those specific matrix elements are fit as well. Rather than fit such individual $\mathbf{k}\cdot\mathbf{p}$-like matrix elements, we chose instead to improve EP-I so that it accurately reproduces the *GW* calculated spin splitting along the Brillouin zone directions which was calculated [6]. The improved

TABLE I. Calculated band structure parameters of bulk GaAs including conduction band energies $E(\Gamma_{6c})$, $E(\Gamma_{7c})$, $E(L_{6c})$, and $E(X_{6c})$ relative to the $E(\Gamma_{8v})$, spin-orbit splittings Δ_0, Δ_0', and Δ_1, and effective masses by two pseudopotentials (EP-I and EP-II). Experimental results at low temperature are taken from Ref. [19] except where noted. The energies are in eV. The k-cubic term γ_i is in eV Å^3.

Property	EP-I	EP-II	Expt.
$E(\Gamma_{6c})$	1.53	1.52	1.52
$E(\Gamma_{7c})$	4.65	4.57	4.49
$E(L_{6c})$	2.36	1.81	1.81
$E(X_{6c})$	1.98	2.02	1.98
$m_e^*(\Gamma_{6c})$	0.066	0.058	0.067
$m_{hh}^*[100]$	0.34	0.31	0.40
$m_{hh}^*[111]$	0.87	0.79	0.90
$m_{lh}^*[100]$	0.093	0.077	0.082
Δ_0	0.341	0.347	0.341
Δ_0'	0.116	0.226	0.174
Δ_1	0.177	0.205	0.213
γ_{CB1}	5.7	8.3	8.5[a], 9[b], 11[b], 17–26[b]
γ_{CB2}	9.6	11.7	
γ_{CB3}	1.7	2.0	
γ_{VB1}	2.6	3.2	
γ_{VB2}	26.6	34.4	
γ_{VB3}	19.0	25.1	

[a]*GW* result; see Ref. [6].
[b]Reference [20].

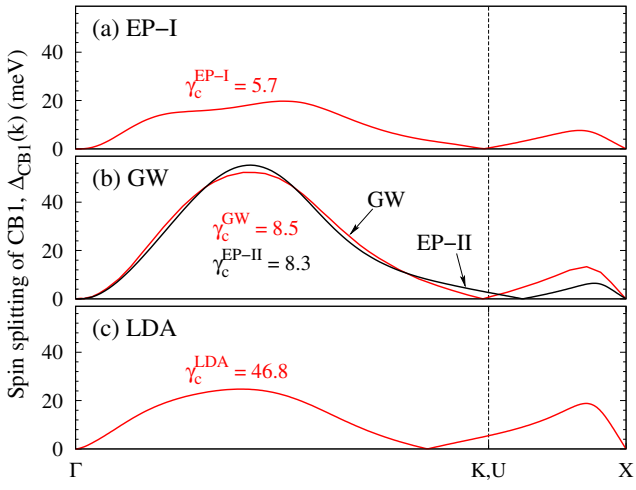

FIG. 1 (color online). Comparison of spin splitting of the lowest GaAs conduction band obtained by (a) our standard empirical pseudopotential (EP-I), (b) *GW* [6] and the improved pseudopotential EP-II, and (c) LDA with projector augmented wave method [21].

GaAs pseudopotential (EP-II) gives results described in Table I and Fig. 1(b). It accurately reproduces band energies, effective masses, and spin splitting. It is obvious from the discussion above that two pseudopotentials (EP-I and EP-II) with equally good fit to energy eigenvalues can give different spin splitting if the underlying momentum and spin-orbit matrix elements are different. This suggests that the small-k behavior of $\Delta_i(\mathbf{k})$ is rather sensitive to the details of the wave functions. Once the crystal potential $V(\mathbf{r})$ (EP-II) is constructed, we employ it to take a glimpse at the full-zone spin splitting which was not observed before.

Small-k behavior.—The fitted k-cubic terms γ of small-k spin splitting at the three lowest conduction bands (denoted CB1, CB2, and CB3) and the three highest valence bands (denoted VB1, VB2, and VB3) are given in Table I. Near Γ, VB1, VB2, and VB3 are usually called, respectively, heavy hole, light hole, and spin-orbit splitting bands, and CB1, CB2, and CB3 represent, respectively, the Γ_{6c}, Γ_{7c}, and Γ_{8c} bands. We note that the k-cubic term γ of VB1 is small but does not vanish. This is contrary to the perturbative prediction [1]. Although the spin-orbit interaction of s-like CB1 band at Γ is induced by indirectly coupling to p-like valence bands [Γ_{8v} (VB1 and VB2) and Γ_{7v} (VB3)] through remote p-like conduction bands [Γ_{8c} (CB3 and CB4) and Γ_{7c} (CB2)], the small-k splitting of CB1 is even larger than that of CB3 and VB1, and is comparable to that of CB2.

Full-zone results.—Once wave vectors shift a bit away from the zone center, the $\mathbf{k}\cdot\mathbf{p}$ model loses its ability to predict the band structure and spin splitting, even qualitatively. Figure 2(a) shows the GaAs band structure (calculated by EP-II) along high symmetry lines. The corresponding spin splitting of the three lowest conduction and highest valence bands is given in Figs. 2(b) and 2(c), respectively.

(i) Rapid changes in spin splitting due to interband coupling.—Figure 2(b) shows that the spin splitting of all the three conduction bands is significantly distorted along Γ to W, and the spin splitting of CB2 and CB3 simultaneously has strong oscillation along Γ to K. Both effects provide evidence for interband coupling within conduction bands. The interband coupling effect can also be found in the spin splitting of CB1 along Γ to K [Fig. 1(a)], where the higher energy spin splitting subband of CB1 is somewhat repelled by same-spin subband of CB2.

(ii) Where in the Brillouin zone does spin splitting peak?—It is commonly believed [1,5] that the largest spin splitting occurs along the (110) direction $\Gamma \rightarrow K$. The reason is that the (110) direction, where spin splitting is allowed [1], is centrally located with respect to the [100] ($\Gamma \rightarrow X$) and (111) ($\Gamma \rightarrow L$) directions along which all or most of the splitting vanishes. In Figs. 2(b) and 2(c) we see that the largest splitting of CB1, VB1, and VB2 occurs along the (210) ($\Gamma - W$) direction, not the (110) direction. Inspecting the spin splitting of VB1 demonstrates that the spin splitting along the (110) direction is negligible compared to the (210) direction. This phenomenon can be seen clearly in a three-dimensional (3D) plot (Figs. 3 and 4) of the spin splitting in Brillouin zone.

(iii) Valence versus conduction band spin splitting.—Figures 3 and 4 show the calculated full-zone spin splitting for the three highest valence bands (right-hand column) and three lowest conduction bands (left-hand column) of GaAs and GaSb, respectively. Each column has two panels for each band. The left-hand panel is a 3D plot in full zone and the right-hand panel is a 2D plot cutting through the zone center and normal to the [001] direction. From the 3D plots in combination with the corresponding 2D partners

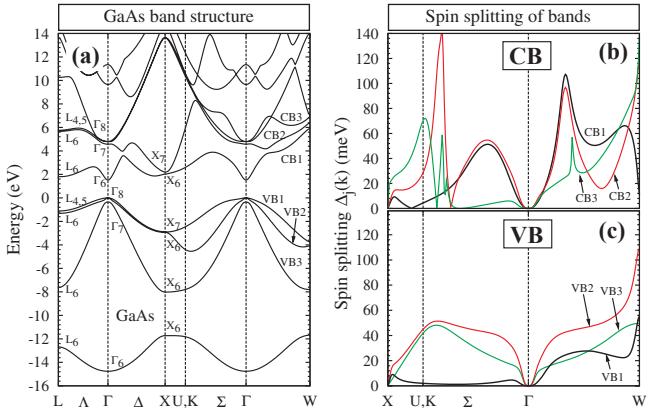

FIG. 2 (color online). (a) GaAs band structure, (b) spin splitting of the three highest valence bands (VB1, VB2, and VB3), and (c) spin splitting of the three lowest conduction bands (CB1, CB2, and CB3).

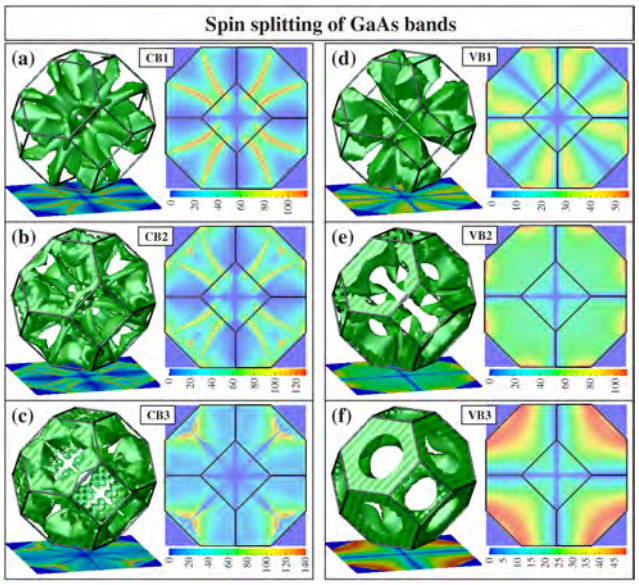

FIG. 3 (color online). Spin splitting of GaAs in the full Brillouin zone for the three lowest conduction bands (a) CB1, (b) CB2, and (c) CB3, and three highest valence bands (d) VB1, (e) VB2, and (f) VB3. Each band has two panels: left-hand panel is a 3D isosurface and right-hand panel is a 2D plane ($k_z = 0$) rendering which is also given at the bottom of left panel. The spin splitting is in meV.

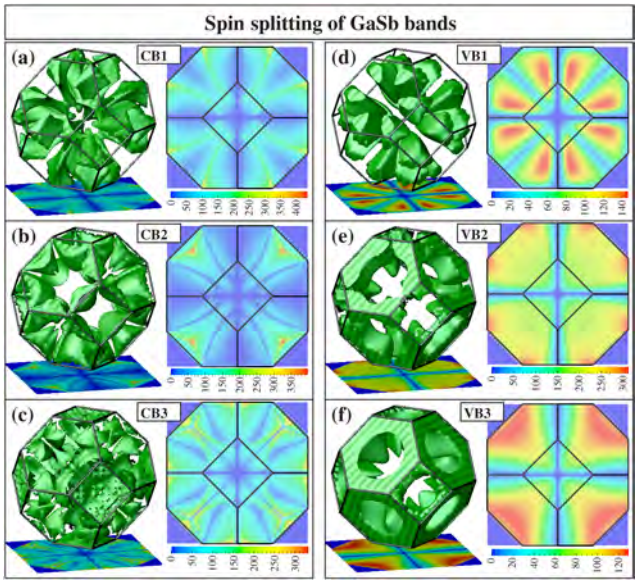

FIG. 4 (color online). Same as Fig. 3 but for bulk GaSb. The pseudopotential calculated GaSb coefficient of k-cubic term of the small-k spin splitting at CB1 is $\gamma_{\mathrm{CB1}} = 68.8$ eV Å^3 which is close to the GW result of 81.8 eV Å^3 [6] relative to linear muffin-tin orbit method value of 108.8 eV Å^3 [5] and experimental value of 185.5 eV Å^3 [5].

we can ascertain that the VB1 and CB1 have largest splitting along (210), not along the (110) direction. If we compare the spin splitting of different bands only along the (110) direction, we would have reached an incorrect conclusion that the spin splitting of VB1 is much smaller than VB2 and VB3. From Figs. 2(c) and 3(d)–3(f), however, we can see that the maximal spin splitting of VB1 is actually comparable to that of VB2 and VB3.

Summary.—We have performed full-zone spin splitting calculations of GaAs and GaSb. We find that (i) the largest spin splitting in the CB1 and VB1 occurs along the (210) direction, not the (110) direction that was previous thought based on limited view of the Brillouin zone (ii) The spin splitting of the upper valence band VB1 is comparable to that of the next two valence bands VB2 and VB3. This has been previously overlooked due to the expectation that the largest spin splitting will occur along the (110) direction. (iii) The interband coupling significantly influences the spin splitting of related bands. To validate our most surprising EPM result—that the spin splitting has a maximum at another area in the Brillouin zone than previously suspected—we performed an independent test, using self-consistent LDA. Our EPM conclusions were corroborated by LDA. For example, LDA predicts that the maximum spin splitting of GaAs CB1 and VB1 along the (210) direction is 140 and 144 meV; however, along the (110) direction it is only 60 and 8 meV, respectively.

This work was funded by the U.S. Department of Energy, Office of Science, Basic Energy Science, Materials Sciences and Engineering, under Contract No. DE-AC36-08GO28308 to NREL.

*Present address: Max Planck Institute for Solid State Research, D-70569 Stuttgart, Germany.
†Corresponding author.
alex zunger@nrel.gov

[1] G. Dresselhaus, Phys. Rev. **100**, 580 (1955).
[2] L. Meier, G. Salis, I. Shorubalko, E. Gini, S. Schön, and K. Ensslin, Nature Phys. **3**, 650 (2007).
[3] Y. Kato, R. C. Myers, A. C. Gossard, and D. D. Awschalom, Nature (London) **427**, 50 (2004).
[4] M. Cardona, N. E. Christensen, and G. Fasol, Phys. Rev. Lett. **56**, 2831 (1986).
[5] M. Cardona, N. E. Christensen, and G. Fasol, Phys. Rev. B **38**, 1806 (1988).
[6] A. N. Chantis, M. van Schilfgaarde, and T. Kotani, Phys. Rev. Lett. **96**, 086405 (2006).
[7] J.-M. Jancu, R. Scholz, G. C. La Rocca, E. A. de Andrada e Silva, and P. Voisin, Phys. Rev. B **70**, 121306(R) (2004).
[8] L. E. Golub and E. L. Ivchenko, Phys. Rev. B **69**, 115333 (2004).
[9] E. E. Vdovin, Y. N. Khanin, L. Eaves, M. Henini, and G. Hill, Phys. Rev. B **71**, 195320 (2005).
[10] R. Magri and A. Zunger, Phys. Rev. B **62**, 10 364 (2000).
[11] P. Piquini, P. A. Graf, and A. Zunger, Phys. Rev. Lett. **100**, 186403 (2008).
[12] J. W. Luo, A. Franceschetti, and A. Zunger, Phys. Rev. B **78**, 035306 (2008).
[13] J. M. An, A. Franceschetti, S. V. Dudiy, and A. Zunger, Nano Lett. **6**, 2728 (2006).
[14] M. Ediger, G. Bester, A. Badolato, P. M. Petroff, K. Karrai, A. Zunger, and R. J. Warburton, Nature Phys. **3**, 774 (2007).
[15] A. Zunger, in *Quantum Theory of Real Materials*, edited by J. R. Chelikowsky and S. G. Louie (Kluwer, Boston, 1996), p. 173.
[16] L. Kleinman and D. M. Bylander, Phys. Rev. Lett. **48**, 1425 (1982).
[17] L. W. Wang, J. Kim, and A. Zunger, Phys. Rev. B **59**, 5678 (1999).
[18] See EPAPS Document No. E-PRLTAO-102-067906 for detailed information on crystal potential including parametrization of pseudopotentials. For more information on EPAPS, see http://www.aip.org/pubservs/epaps.html.
[19] *Semiconductors: Group IV Elements, IV-IV and III-V Compunds*, edited by U. Rössler, Landolt-Börnstein, New Series, Group III, Vol. 41, Pt. a (Springer-Verlag, Berlin, 2001).
[20] J. J. Krich and B. I. Halperin, Phys. Rev. Lett. **98**, 226802 (2007); experimental values in literature are collected in supplementary information.
[21] G. Kresse and J. Furthmüller, Phys. Rev. B **54**, 11 169 (1996); G. Kresse and D. Joubert, *ibid.* **59**, 1758 (1999).